Studies of broad emission line profiles in QSOs - I. Observed, high-resolution profiles

Mon. Not. R. astr. Soc. (1984) 207, 73–98

Studies of broad emission line profiles in QSOs – I. Observed, high-resolution profiles

Belinda J. Wilkes *Steward Observatory, University of Arizona, Tucson, Arizona 85721, USA*

Received 1983 July 4; in original form 1983 January 28

Summary. High-resolution spectra of nine high-redshift QSOs are presented. The various emission line profiles of each QSO are intercompared in order to gain information on the kinematics of the emitting gas in the broad-line region (BLR). A small number of these profiles, which are either typical of the sample or of special interest, are presented diagrammatically. A full presentation of all the line profiles can be obtained from the author. The main results are summarized and their implications regarding the kinematics of the BLR discussed.

1 Introduction

It is generally believed that the broad emission lines that characterize the spectra of QSOs originate in a region of photoionized gas, optically thick to the Lyman continuum, surrounding a central source of non-thermal radiation. The subject has been extensively reviewed by Davidson & Netzer (1979); detailed recent calculations are presented by Kwan & Krolik (1981).

The large velocity widths of the lines (full-width at half-maximum, FWHM ~ 5000 km s^{-1}) are believed to be caused by large-scale motions of the emitting gas and thus the shapes of the line profiles provide a global picture of the spatial and dynamical distributions of the gas. Few studies of these profiles have been attempted, mainly due to the large amount of telescope time required to obtain high-quality, high-resolution spectral data for faint objects. Low-resolution spectra indicate that the line profiles have similar shapes and velocity widths (Baldwin 1975; Baldwin & Netzer 1978) and that their profiles are approximately logarithmic (Blumenthal & Mathews 1975). Since the emission lines cover a large range of ionization states, these results imply that gas having highly discrepant ionization conditions exists in similar regions of the BLR, placing important constraints on photoionization models. However, the accuracy of these comparisons is low and, in addition, all the emission lines, with the possible exception of C IV, are blended with weaker features (e.g. Wills, Netzer & Wills 1980). The reliability of conclusions based upon low-quality data where the individual features cannot be discerned is highly questionable.

The covering factor of the BLR gas has been estimated by several authors to be small

($\epsilon \sim 5$–10 per cent) (Baldwin & Netzer 1978; Carswell & Ferland 1980; Smith *et al.* 1981), implying that the gas is contained in a large number of independently radiating small clouds surrounded by a sparse, low-density intercloud medium (ICM) (Davidson 1972). Searches for structure in the line profiles have so far proved negative, placing an observational lower limit on the number of clouds at $\sim 10^4$ (Atwood, Baldwin & Carswell 1982).

It is clear that, due to the lack of data, knowledge of all but the physical conditions of the BLR gas is very limited. It is essential to the future of studies of the QSO BLR that the emphasis of observational programs be shifted from quantity to quality, enabling definite statements to be made about the emission-line profiles as opposed to hand-waving generalizations. This paper takes a step in this direction by presenting high-resolution spectral data (~ 1–2 Å) for a sample of nine high-redshift QSOs. The *S/N* of these data is on the whole superior to that previously available in the literature. The ultraviolet emission lines discussed here span the intrinsic wavelength region from O VI λ 1034 at the blue extreme to C III] λ 1909 at the red. This range will be extended to lower redshift, thus including Mg II λ 2798, in a later paper. The observational details are described in Section 2 and in Section 3 the spectra are presented along with notes on each individual QSO. The method for analysing and intercomparing these profiles and the effect of possible errors in the estimated level and slope of the continuum emission are considered in Section 4. In Section 5 the results of intercomparing the various line profiles within each object are described.* Finally, these results and possible interpretations are discussed (Section 6) and the main results and suggestions for important follow-up observations are summarized (Section 7).

2 Observations

Spectra were obtained in 1979 November, 1980 April and 1981 September using the image photon counting system (IPCS) (Boksenberg 1972, 1978) on the RGO spectrograph at the

Table 1. Wavelength range and dispersion obtained with echellette.

Order	Wavelength range	Dispersion (Å/ch)
4	5400–7060	1.0
5	4400–6000	0.8
6	3650–4900	0.67
7	3500–4200	0.57*

* Response relatively poor.

f/8 Cassegrain focus of the Anglo-Australian telescope. The spectrograph was used with a 150 gpm grating blazed at 2.6 μm and a grism cross-disperser (40 gpm on a 2°.43 UBK7 prism) to separate the orders. Useful information was obtained for the object and sky spectra simultaneously in the fourth and seventh orders, using apertures separated by ~ 20 arcsec. The wavelength range and dispersions obtained are summarized in Table 1. A 225 μm (1.5 arcsec) slit was used, matching the detector resolution of three pixels. Sky and object positions were interchanged at 1500 s intervals, in order to correct for any asymmetries in the system response, and comparison arc spectra for wavelength calibration were recorded after each pair of integrations.

The data were collected in a two-dimensional array of 2030 spectral channels by 90 spatial increments and subsequently extracted and analysed using the SERC STARLINK VAX

* Due to the large numbers involved, only 'typical' or particularly interesting profiles are presented in this paper. For a full presentation of all the profile comparisons, please apply to the author.

Table 2. Observational details.

QSO	R A	Dec.	$\bar{z}$	m_v*	DATE OF OBSERVATION	DWELL TIME(S)	REF.
Q0000-398	00 00 30.3	-39 48 57	2.830	18.8	NOV 79	3000	1,2
Q0207-398	02 07 24.3	-39 53 50	2.813	17.5	NOV 79	3000	1,2
0304-392	03 04 18.8	-39 17 34	1.965	17.6	SEP 81	13000	
Q1101-264†	11 01 00.0	-26 29 08	2.144	16.0	-	-	3,4
" (ECH)					APR 80	6000	
1331+170	13 31 10.0	+17 04 20	2.084	16.0	APR 80	12000	5,6,7
1559+089	15 59 57.8	+08 53 53	2.269	-	SEP 81	4000	
2044-168	20 44 31.0	-16 50 12	1.937	16.9	SEP 81	16000	
					Lyα	CIV	
Q2204-408†	22 04 33.1	-40 51 39	3.170	17.5	- 12000	16000	3,8
2212-299	22 12 25	-29 59 20	2.700	17.5	SEP 81	8000	

1. Osmer & Smith (1976)
2. Whelan, Smith & Caswell (1979)
3. Osmer & Smith (1977)
4. Carswell *et al.* (1982)
5. Baldwin & Netzer (1978)
6. Strittmatter *et al.* (1973)
7. Carswell *et al.* (1975)
8. Osmer (1979)

* From Hewitt & Burbidge (1980).
† Data obtained by Boksenberg, Carswell, Smith & Whelan, details given in quoted reference.

computer at the Institute of Astronomy, Cambridge. The extraction programs used were similar to those used by Carswell *et al.* (1975), developed then for a similar spectrograph system. The data were corrected to a relative flux scale using standard star observations of white dwarfs for which Oke (1974) has published spectrophotometric data. Details of the objects observed are listed in Table 2 along with their mean redshift, visual magnitude and total exposure time.

3 The spectra

The spectra are displayed in order of right ascension in Fig. 1; they are plotted on an arbitrary scale of flux per unit frequency interval versus wavelength in Å. This scale is convenient for profile work since it approximates to energy per unit velocity interval. Prior to isolating and comparing the line profiles (described in Sections 4 and 5) various parameters characterizing each of the emission lines were measured, these are given in Table 3 for each QSO as follows: column 1, object name; column 2, observed mean redshift;* column 3, name of emission line; column 4, redshift of the peak; column 5, the effective rest wavelength of the peak (with respect to the mean QSO redshift); column 6, rest frame wavelength of the point of reflection (see Section 4); column 7, the flux in the line relative to that of the C IV λ 1549 emission feature; column 8, notes; column 9, references.

3.1 NOTES ON INDIVIDUAL OBJECTS

Q0000 – 398

There is no detectable feature at 1400 Å in this spectrum, which is unusual particularly when the low-ionization lines are relatively strong. The Lyα λ 1216 and C IV λ 1549 profiles were tested for asymmetry and, in both cases, none was detectable (see also Wilkes & Carswell 1982, hereafter WC82). When compared with C IV, the O VI λ 1034 line was found to have a

* This was calculated from the positions of all the observed emission lines with the exception of those known to be blended and also the low-ionization lines, e.g. O I λ 1034 which have been observed to be redshifted relative to the high-ionizaton lines and Lyα λ 1216 (Gaskell 1981, 1982; Wilkes 1982).

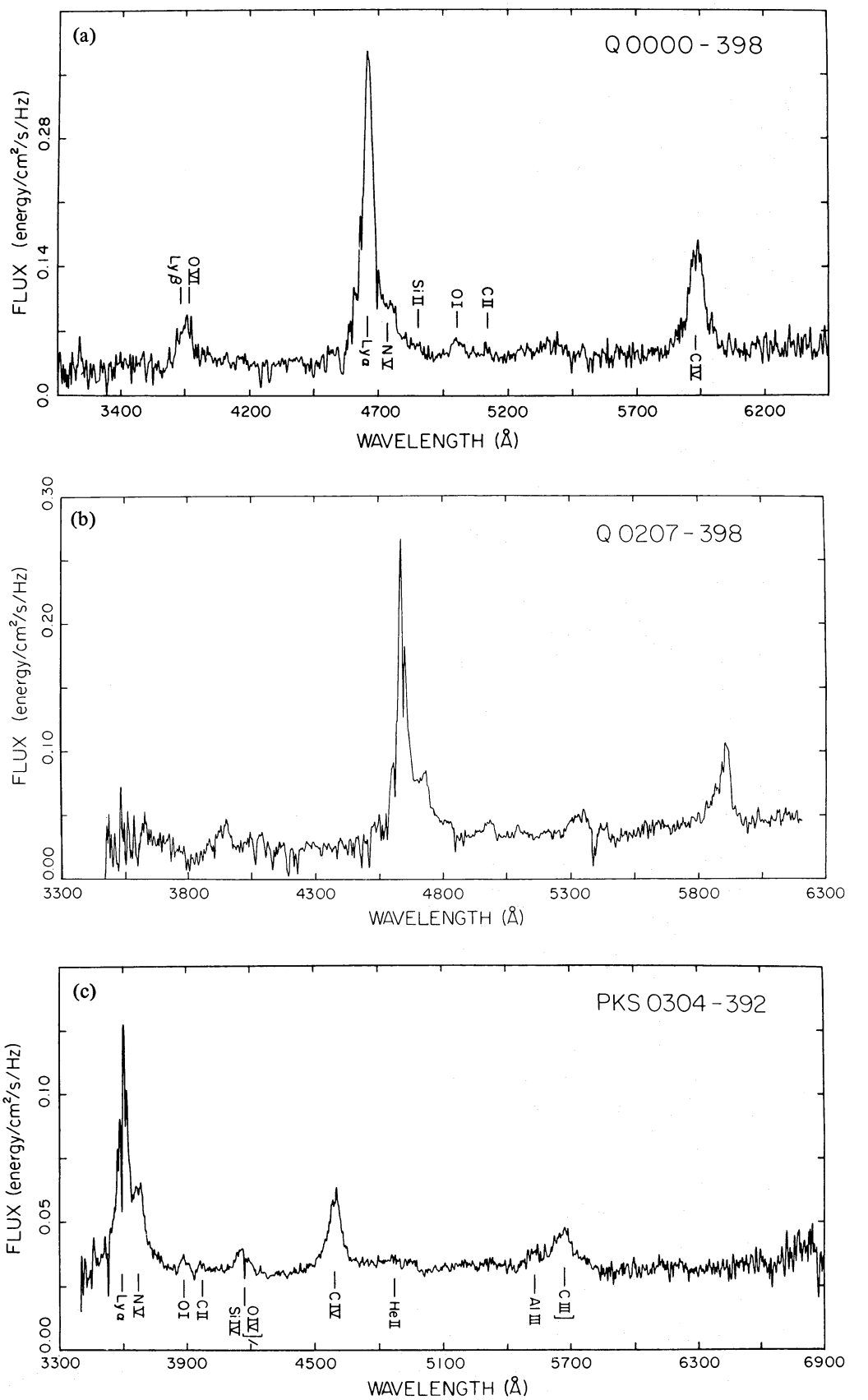

Figure 1. High-resolution spectra of the QSOs in order of right ascension plotted on an arbitrary scale of flux per unit frequency interval versus wavelength in Å. Expected positions of emission lines discussed in this paper are indicated on their first appearance.

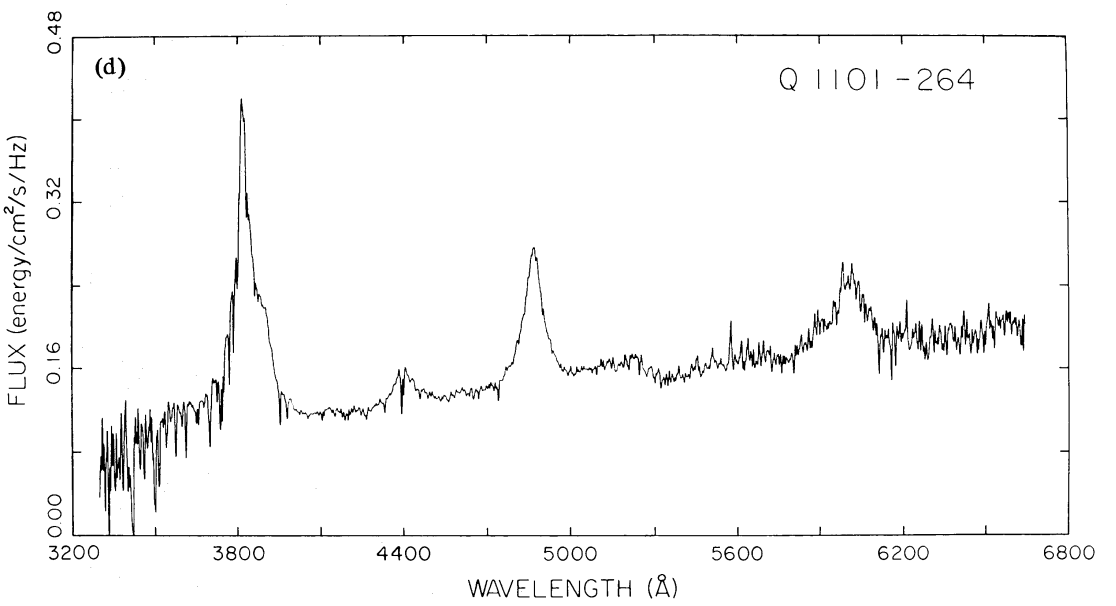

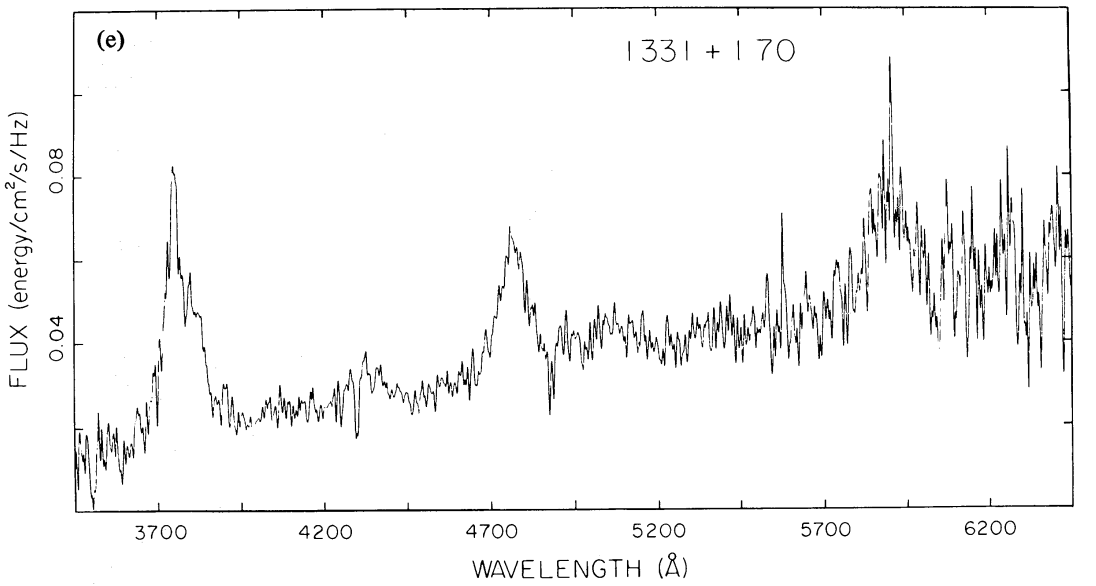

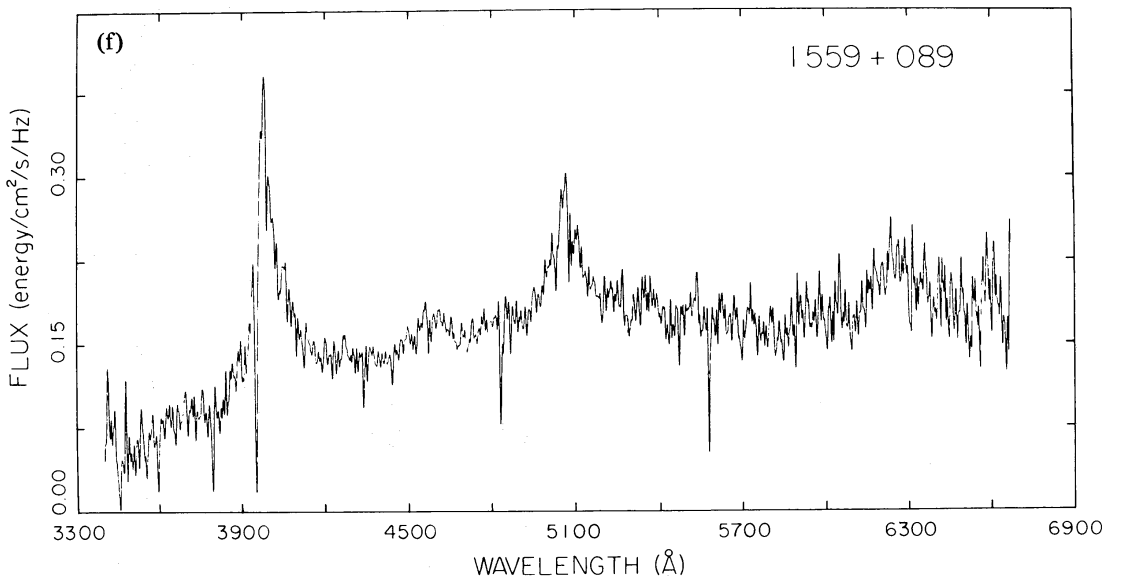

Figure 1 – *continued*

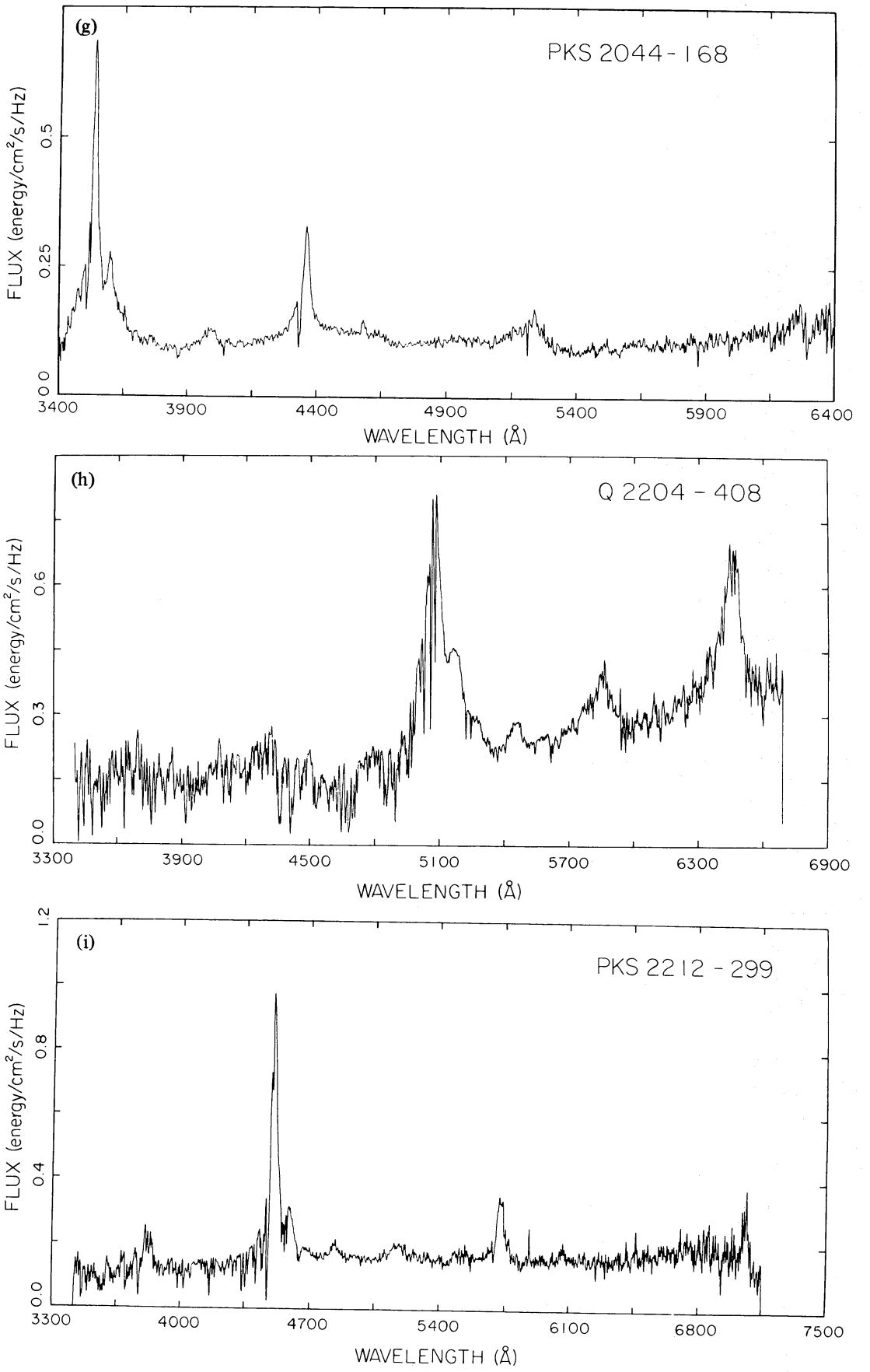

Table 3. Characteristics of emission lines.

OBJECT	$\bar{z}$	LINE	z_p	λ_{eff}	λ_{ref}	FWHM/kms^{-1}	Flux rel. CIV	Notes	References
Q0000-398	2.830	OVIλ1034	2.826	1032.4	-	3940	0.7	-	1,2,3,10
		Lyαλ1216	2.831	1215.9	1216.1	3410	3.9	Symmetric	
		NVλ1240	2.828	1239.4	-	3410	0.5	-	
		OIλ1304	2.841	1307.3	-	3120	0.1	-	
		CIIλ1335	2.831	1335.2	-	1060	0.03	-	
		CIVλ1549	2.830	1549.1	1549.0	3640	1.0	Symmetric	
Q0207-398	2.813	OVIλ1034	2.813	1033.6	1034.7	3730	0.5	Blue skew	1,2,3,10
		Lyαλ1216	2.814	1216.1	1216.2	2460	5.9	Symmetric	
		NVλ1240	2.813	1240.2	-	5330	1.4		
		SiIIλ1264	-	-	-	-	0.4		
		OIλ1304	2.821	1306.3	-	2540	0.2		
		CIIλ1335	2.815	1335.7	-	940	-		
		OIV]/SiIVλ1400	-	1397.3	-	3990	0.3		
		CIVλ1549	2.813	1549.2	1548.5	2390	1.0	Blue skew	
0304-392	1.965	Lyαλ1216	1.961	1214.2	-	4080	> 3	∿ Blue skew	4
		NVλ1240	1.967	1240.8	-	4240	∿ 1.3		
		SiIIλ1264	-	-	-	-	∿ 0.2		
0304-392 (cont.)	1.965	OIλ1304	1.979	1309.6	-	2410	0.3		
		CIIλ1335	1.971	1337.6	-	1600	0.04		
		CIVλ1549	1.966	1549.4	1550.0	4570	1.0	Blue skew	
		CIII]λ1909	1.965	1908.6	1909.2	6310	0.5	Symmetric	
Q1101-264	2.144	Lyαλ1216	2.141	1214.4	1214.4	4400	2.5	∿ Symmetric	7,8,10
		NVλ1240	2.147	1241.1	-	5690	0.6		
		SiIIλ1264	-	-	-	-	0.2		
		OIV]/SiIVλ1400	-	1400.8	-	5450	0.3		
		CIVλ1549	2.145	1549.6	1549.4	4560	1.0	Symmetric	
		CIII]λ1909	2.144	1909.0	1910.5	6050	0.1	Blended in blue wing	

1984MNRAS.207...73W

Table 3 – *continued*

OBJECT	$\bar{z}$	LINE	z_p	λ_{eff}	λ_{ref}	FWHM/kms^{-1}	Flux rel. CIV	Notes	References
1331+170	2.084	Lyαλ1216	2.086	1216.6	1216.3	4880	2.5	Symmetric	9,10,11,12
		NVIλ1240	2.088	1241.9	-	5100	0.7		
		OIV]/SiIVλ1400	-	1402.1	-	6390	0.3		
		CIVλ1549	2.077	1545.4	1546.2	5590	1.0	Symmetric	
		CIII]λ1909	2.091	1913.1	-	-	-		
1559+089	2.269	Lyαλ1216	2.269	1215.7	1215.7	4530	2.5	Symmetric	13
		NVλ1240	2.273	1241.7	-	5250	0.8		
		SiIIλ1263	-	-	-	-	0.2		
		OIλ1304	2.273	1305.3	-	1430	-	noisy	
		OIV]/SiIVλ1400	-	1399.5	-	4920	-		
		CIVλ1549	2.268	1548.5	1549.5	4380	1.0	∿ blue skew	
		CIII]λ1909	2.266	1907.0	-	-	-		
2044-168	1.937	Lyαλ1216	1.933	1213.8	1213.8	3020	5.6		14, 15
		NVλ1240	1.939	1241.1	-	3050	0.8		
		OIλ1304	1.942	1305.8	-	1880	-		
		OIV]/SiIVλ1400	-	1399.4	-	4380	0.2		
		CIVλ1549	1.939	1549.9	1550.2	2440	1.0	Blue skew	
		HeIIλ1640	1.936	1640.1	-	1060			
		CIII]λ1909	1.937	1908.8	1909.2	6050	0.4	Blue skew	
Q2204-408	3.170	CIIIλ977	3.172	977.7	-	960	-		4,7,16,10
		OVIλ1034	3.158	1030.7	-	6820	-	Blue skew	
		Lyαλ1216	3.171	1216.4	1216.1	4200	2.8	Blue skew	
		NVλ1240	3.164	1238.4	-	6440	0.1		
		SiIIλ1264	-	-	-	-	0.02		
		OIλ1304	3.182	1307.5	-	2980	0.1		
		OIV]/SiIVλ1400	-	1404.9	-	4270	0.4	Blue skew	
		CIVλ1549	3.169	1547.6	1548.7	4270	1.0	Blue skew	

2212-299	2.700	Lyγλ973	2.703	973.2	-	1240	-	6, 10
		OVIλ1034	2.687	1029.7	-	5260	-	
		Lyαλ1216	2.702	1216.5	1216.2	2670	-	
2212-299 (cont)	2.700	NVλ1240	2.698	1239.5	-	4250	∿ 1.2	
		SiIIλ1264	-	-	-	-	∿ 0.2	
		OIλ1304	2.708	1306.2	-	2550	0.2	
		OIV]/SiIVλ1400	-	1400.5	-	4460	0.3	
		CIVλ1549	2.700	1548.9	1549.7	2670	1.0	∿ Blue skew
		HeIIλ1640	2.700	1640.3	-	1630	-	
		CIII]λ1909	2.699	1908.1	1907.7	1530	0.4	Symmetric

1. Smith (1976)
2. Osmer & Smith (1976)
3. Whelan, Smith & Carswell (1979)
4. Osmer & Smith (1980)
5. Burbidge & Kinman (1966)
6. Jauncey *et al.* (1978)
7. Osmer & Smith (1977)
8. Carswell *et al.* (1982)
9. Baldwin *et al.* (1973)
10. Wilkes & Carswell (1982)
11. Carswell *et al.* (1975)
12. Baldwin & Netzer (1978)
13. Hazard (private communication)
14. Peterson *et al.* (1976)
15. Weymann *et al.* (1979)
16. Osmer (1979)

significant Lyβ λ 1026 contribution in its red wing: $I(\text{Ly}\beta)/I(\text{O VI}) \sim 0.31$, i.e. $I(\text{Ly}\beta)/I(\text{Ly}\alpha) \sim 0.06$ (see Section 5). Measurements of the C II λ 1335 feature are inaccurate due to its weakness.

Q0207 – 398

The C IV λ 1549 profile has a pronounced blue asymmetry and the features O VI λ 1034 and N V λ 1240 also appear asymmetric in the same sense, although contamination by absorption lines in the first case and blending with Lyα in the second prevent a detailed comparison. It should also be noted that Osmer & Smith (1976) report the wavelength of C IV λ 1549 to be 16 Å bluer than that estimated here; this discrepancy is likely to be the result of combining their low resolution (~ 40 Å) with the blue asymmetry of the emission line. C II λ 1335 is significantly narrower at FWHM than the other lines and does not share the relative redshift of O I λ 1304.

0304 – 392

The Lyα λ 1216 emission feature is heavily contaminated by absorption lines preventing detailed study of the profile. Superposition in the C IV velocity space suggests the Lyα peak is at a lower velocity and its blue wing is stronger than that of C IV. The C IV profile has a blue asymmetry similar to but less pronounced than that in Q0207 – 398. In addition, blends of Fe II emission, as identified by Gaskell (1981), are present in the spectral region between C IV and He II λ 1640. The C III] λ 1909 profile is apparently symmetric but there is a suggestion of emission in the extreme blue wing at 1864 Å (rest frame), which may be analogous to that found in Q1101 – 264 and 2044 – 168 (see below). There are also two apparent weak, narrow emission lines in the blue wing of Lyα at wavelengths of 1168 and 1185 Å in the rest frame of the QSO. These features have so far not been positively identified.

Q1101 – 264

The C IV profile in this object is symmetric to well within the error margin. The Lyα λ 1216 profile has a marginal blue skew but this is probably due to the large discrepancy between the wings of the C IV and Lyα profiles which causes overestimation of the N V contribution to the blend (see WC82). Blends of Fe II emission are once again present redward of the C IV profile; the continuum level was estimated using the spectral region redward of this emission. The C III] λ 1909 profile has a partially resolved emission feature blended into its blue wing and centred ~ 1872 Å in the rest frame of the QSO (see Section 5).

1331 + 170

The *S/N* in this spectrum is not very good, particularly to longer wavelengths around the C III] λ 1909 emission line. Unusual shifts are present: the C IV line peak is blueshifted with respect to Lyα and C III]. This is a reliable result for Lyα and C IV but the estimated position of C III] is inaccurate. Baldwin & Netzer (1978) presented a low-resolution spectrum. They found the C IV and C III] profiles to be similar to within the *S/N* of their data and reported no shift.

1559 + 089

The spectrum is fairly rich in absorption lines. In particular there is an almost black, relatively broad line ~ 2000 km s^{-1} blueward of the peak of Lyα and a possible, but noisy, counterpart at the same redshift in the C IV profile. Both emission line profiles appear to have an extended blue wing. The poor *S/N* of the data facilitated only rough estimates of the positions of O I λ 1304 and the 1400 Å feature.

2044 – 168

The C IV emission line profile has a significantly enhanced and extended blue wing, similar to that of C IV in Q0207 – 398. C III] is again blended with a weak feature at ~ 1871 Å (rest frame). He II λ 1640 is unusually strong, relatively narrow and blueshifted ~ 300 km s^{-1} with respect to the C IV peak. Fe II emission is present longward of C IV, though it is weaker in this spectrum than in either of the two previously reported. In addition, a strong, high-ionization absorption system is present at a redshift of 1.92 including Lyα, C IV and possibly N V lines.

The discrepancy between the profiles of Lyα and C IV is so great that it is not possible to deblend Lyα and N V. The Lyα profile appears to consist of an exceptionally broad component with a narrower component superposed, the usual shape being accentuated by the presence of strong absorption lines on both sides of the peak. In Fig. 2(a) and (b) the real and 'cleaned' (see Section 4) profiles of Lyα and C IV respectively are displayed, in Fig. 2(c) the two cleaned profiles are superposed in the same velocity space, arbitrarily scaled to match their red wings. The difference in shape is clear, the broad Lyα wings extending in both directions beyond those of C IV. The cores of the two lines have similar widths implying that a possible explanation of the profile anomaly is the superposition of a very broad Lyα emission component upon a 'regular' profile with a similar shape to C IV. This broad component may originate in a high velocity, low-ionization component of gas. Whatever its origin it is, to the best of my knowledge, unlike any profile observed to date in a QSO spectrum.

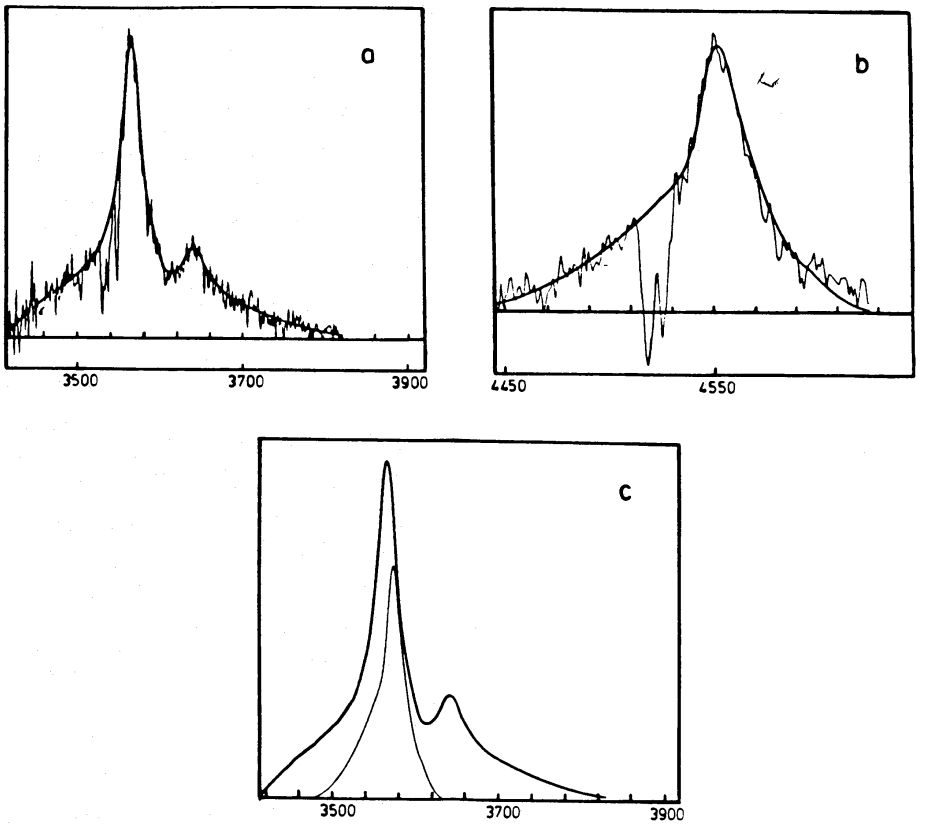

Figure 2. The observed profiles of (a) Lyα and (b) C IV for PKS 2044 – 168 with the cleaned versions superposed. (c) Superposition in the same velocity space of the Lyα (reinforced) and C IV profiles, arbitrarily scaled to match their near-red wings.

Q2204 – 408

This QSO is very rich in absorption lines but at the high-resolution of these data the emission line profiles are clearly visible. Lyα, C IV and O IV]/Si IV λ 1400 have an unusual, pronounced blue asymmetry (WC82). O VI λ 1034 is heavily absorbed, particularly in the red wing, but also appears to share this asymmetry. The N V profile after being deblended from Lyα appears fairly symmetric although Si II λ 1263 emission may be present in the red wing. The O I λ 1304 feature is also roughly symmetric and is redshifted a typical 860 km s^{-1} with respect to the other emission lines.

2212 – 229

The high-resolution data presented here reveal a rich absorption line spectrum. The Lyα profile is sufficiently contaminated that the detailed shape cannot be discerned. The C IV profile has a slightly enhanced blue wing and Lyα, after deblending N V and Si II λ 1263, appears to have a similar asymmetry. Deblending of the O VI/Lyβ profile using C IV led to an estimated intensity ratio $I(\text{Ly}\beta)/I(\text{O VI}) \sim 0.46$. There is also a possible weak emission feature at ~ 3603 Å, in the midst of the Lyα forest of absorption lines, whose wavelength of 973.2 Å (rest frame) suggests an identification as Lyγ λ 973. Its intensity relative to Lyβ is ~ 0.5. The absorption contamination of Lyα allows only rough limits to be placed on the relative intensity of the other two Lyman lines: $0.06 \sim I(\text{Ly}\beta)/I(\text{Ly}\alpha) < 0.1$ (see Section 5 for further discussion).

4 Analysis of the emission line profiles

The emission line profiles available in this sample vary widely in their *S/N* properties and in the number and strength of the narrow absorption lines present. Intercomparison of such profiles prove both confusing and impractical. Gaussian smoothing, after removing obvious absorption lines, may be used to produce uniform *S/N* properties but in many cases this results in significant degradation in the resolution across the profiles and alteration of their shape. Consequently a quadratic interpolation routine was invoked to generate a number of fits through short sections of the observed emission line profile allowing for contaminating absorption lines. These fits were then combined to produce a 'clean' version of the profile without any degradation of resolution. The 'cleaned' profiles were used as far as possible in the subsequent profile comparisons. But, since the routine is somewhat subjective, superposition of clean and original features was always used in conjunction so that the reliability of the results could be determined.

The cleaned profiles of each QSO were compared by superposition in the same velocity space using the method originally introduced by Baldwin & Netzer (1978). In cases where the observed feature was known to be a blend of two or more emission lines, a synthetic blend was generated by superposing a second, unblended feature in the velocity space of each component of the observed blend. The relative strengths of each contributor to this synthesis were varied to obtain an optimal fit to the observed profile, determined by minimizing the residual between the two. Thus, an estimate of the relative contributions of each component was obtained, dependent upon the degree of similarity between the intrinsic profiles of the various lines involved. The nature of problems encountered during deblending due to discrepancies between the constituent profiles, with specific reference to deblending N V and Lyα emission, were discussed in an earlier paper (WC82).

One of the greatest problems in comparing the emission profiles in the spectrum of a QSO is in estimating the accuracy of the continuum level adopted in each case. The main limitations on its accurate positioning are: the noise level; the possible presence of weak

absorption features which are indistinguishable from the noise; and the presence of weak, blended emission features, mainly due to Fe II, which vary greatly in strength from object to object. Considering each of these limitations in turn:

(i) At the resolution of this data sample the majority of the narrow absorption lines are well resolved and those that are above the noise level can be allowed for unambiguously. Unfortunately, an assessment of the number and effect of those that are weak and lost in the noise depends solely upon statistical arguments. Such features may be numerous enough to depress the apparent continuum, particularly in the blue wing of Lyα owing to the high density of narrow absorption lines in the Lyα forest.

(ii) The most commonly considered contaminating features are blends of Fe II emission. These have been widely discussed by many authors (e.g. Phillips 1978a, b; Grandi 1981; Collin-Souffrin *et al.* 1979; Peterson, Foltz & Byard 1981; Wills *et al.* 1980). Fe II emission is generally believed to be stronger in radio-quiet QSOs; however, it is clearly present redward of C IV in three QSOs, 0304 – 392, Q1101 – 264 and 2044 – 168, in this sample (Fig. 1), two of which are radio-selected. Thus the possibility of substantial emission cannot be ignored even for radio-loud members of the sample.

In addition, C III] is probably contaminated in its blue wing by emission attributed to Si III] λ 1892, Al III λ 1858, Fe II λ 1860 or some combination of all three (Wills *et al.* 1980; Gaskell 1981; Section 5 of this paper). The presence of other weak features which remain indiscernible from the noise and have not been detected to date is likely since the *S/N* of QSO spectra is rarely high.

(iii) The properties of photon noise are well understood and thus quantitative estimates of the errors from this source could be made. However, without similar assessment of the effect of weak absorption and emission features, which are likely to dominate, these are worthless.

The accuracy of the continuum level around each emission line profile depends upon factors whose relative effects cannot be estimated or quantified in any consistent manner. The problem remains that an incorrect height and/or slope for the chosen continuum level in the region of an emission line may alter the apparent shape of the line profiles. In particular, a slight variation in slope may introduce an asymmetry into the profile or detract from one already present. A study of the magnitude and character of any erroneous results likely to be

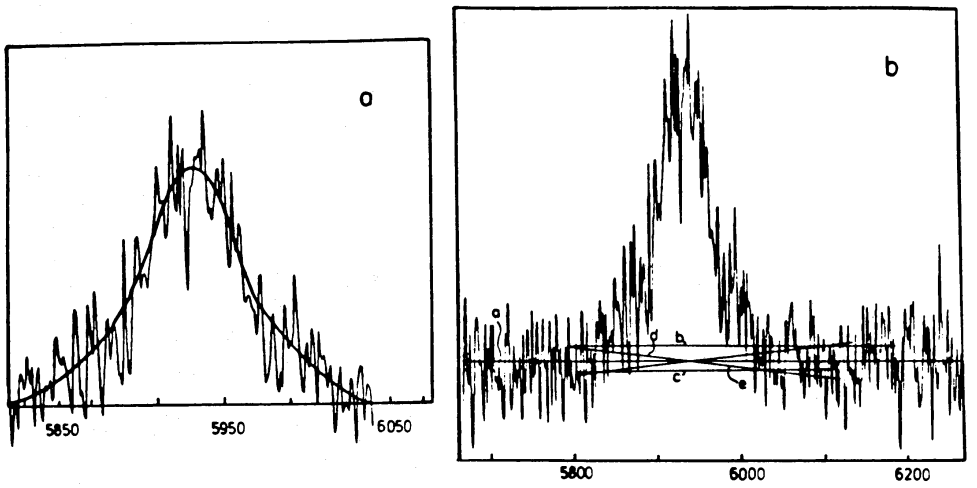

Figure 3. (a) The C IV profile of Q0000 – 398 with a cleaned version superposed. (b) The spectrum in the region around C IV with five versions of the continuum level superposed.

introduced into the profile comparisons was performed utilizing the C IV profile from Q0000 – 398, which is displayed, with smoothed version superposed, in Fig. 3(a). The *S/N* properties across the profile are typical of the sample as a whole and the feature has no notable peculiarities. The optimum estimate of the continuum level is made by fitting a second-order polynomial through as large an expanse of continuum on either side of the line as possible. There are four extremes around this preferred level at which a continuum could be set, these are illustrated in Fig. 3(b) and detailed in the caption to this figure. The cleaned version of the feature was isolated from the continuum emission adopting each of these levels in turn yielding five versions of the same line profile. These isolated profiles were then compared with one another to investigate the magnitude of the resulting discrepancies and reflected to study the induced degree of asymmetry (see WC82).

The following conclusions were reached as a result of this study:

(i) Inaccuracies in the continuum level and slope combined cause a mean error of ~ 3 per cent, normalized to the peak intensity, in the flux level in the main body of the profile, rising to ~ 5 per cent in the extreme wings.

(ii) Asymmetries yielding discrepancies of up to ~ 4 per cent between the two wings of a profile may be caused by erroneous continuum levels.

These errors are within the level of the noise in all the profiles in this sample and thus are not considered to be a source of substantial systematic errors.

5 Profile comparisons

The most important factors in determining the observed shape of a particular line profile emitted by a system of radiating gas clouds are: the velocity distribution of the clouds; their number density distribution; the intensity of radiation emitted by each as a function of viewing angle; and any attenuation due to dust. All these quantities may be a function of the distance of a cloud from the central ionizing source of radiation. Clearly the velocity distribution and number density of clouds are parameters which are common to every species of emission line. Thus, any differences between their final line profiles would be the result of a radial dependence in their radiation intensities, possibly caused by varying photoionization conditions and/or high line, continuum or dust opacities. Thus, knowledge of the relative shapes of the observed profiles combined with photoionization model calculations of emitted intensity as a function of radius, can yield information or the kinematics and dynamics of the clouds. A theoretical approach to this problem will be discussed in a later paper in this series.

In this section general results of the profile comparisons will be outlined, peculiarities found in individual objects having been described in Section 3.

5.1 C IV λ 1549 AND LY α λ 1216

In eight of the nine QSOs for which this comparison was performed, the Lyα profile showed a relatively stronger peak and more extended wings than the corresponding C IV profile. This has already been noted for those QSOs utilized in the investigation of Lyα asymmetry (WC82) and is apparent in the figures shown there. Although the difference is sometimes only marginally significant in an individual case, the presence of a trend is assured. The comparison of C IV and Lyα in Q0000 – 398 is shown in Fig. 4(a) as an illustration; superposition of cleaned and orignal profiles can be found in Fig. 3(a) and WC82 for C IV and Lyα respectively.

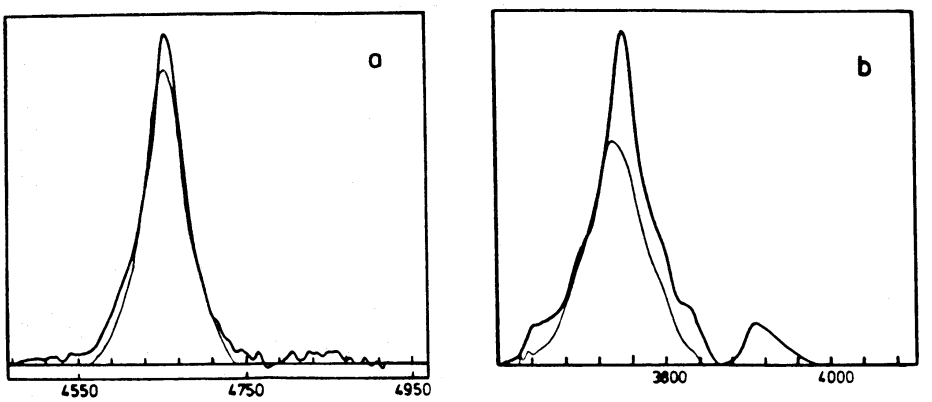

Figure 4. (a) Superposition in the same velocity space of the Lyα (reinforced) and C IV profiles for Q0000 – 398. (b) The same comparison for the profiles of 1331 + 170.

The exceptional profiles are those of 1331 + 170, for which the C IV profile, despite being symmetric, has an apparent peak which is blueshifted ~ 900 km s^{-1} relative to the Lyα peak (WC82). In Fig. 4(b) the superposition of C IV and isolated Lyα cleaned profiles, in the Lyα velocity space, is displayed with the vertical scale fixed arbitrarily to match the blue wings. The shift between the two peaks is apparent and there is also evidence that the red wing of the Lyα profile is relatively stronger and more extended.

5.2 REDSHIFT OF LOW-IONIZATION LINES

The low-ionization lines found in this region of the spectrum are O I λ 1304 and C II λ 1335. Both these lines are weak, C II being the weaker, but they are clearly visible in several spectra of the present sample. The positions of O I λ 1304 and C II λ 1335 are tabulated in Table 4 as follows: Column 1, name of QSO; column 2, mean redshift; columns 3 and 5, peak redshift of O I and C II respectively; column 4 and 6, corresponding shift of the line peak in velocity units. All seven of the available O I lines are redshifted and the mean, ~ 740 km s^{-1}, is in good agreement with the findings of Gaskell (1982). Two of the three C II lines are approximately at rest and the third is redshifted by ~ 610 km s^{-1}, substantially lower than the shift of O I in the same QSO (1420 km s^{-1}).

Since both the emission lines are weak, profile comparisons are not very accurate. In Fig. 5(a) the O I profile of Q0000 – 398 is displayed with the cleaned version superposed. (For C IV see Fig. 3a.) In Fig. 5(b) O I is superposed upon C IV (reinforced) in the same velocity space, the relative strengths being arbitrarily adjusted to match the red wings as far as

Table 4. Shifts of O I λ 1304 and C II λ 1335 emission lines relative to the mean redshift, $\bar{z}$ (z_p = redshift of line peak; Δv = velocity shift relative to z).

		OIλ1304		CIIλ1335	
QSO	$\bar{z}$	z_p	Δv(kms^{-1})	z_p	Δv(kms^{-1})
Q0000-398	2.830	2.841	860	2.831	0
Q0207-398	2.813	2.821	630	2.815	160
0304-392	1.965	1.979	1420	1.971	610
1559+089	2.269	2.273	370	-	-
2044-168	1.937	1.942	510	-	-
Q2204-408	3.170	3.182	860	-	-
2212-299	2.700	2.708	650	-	-

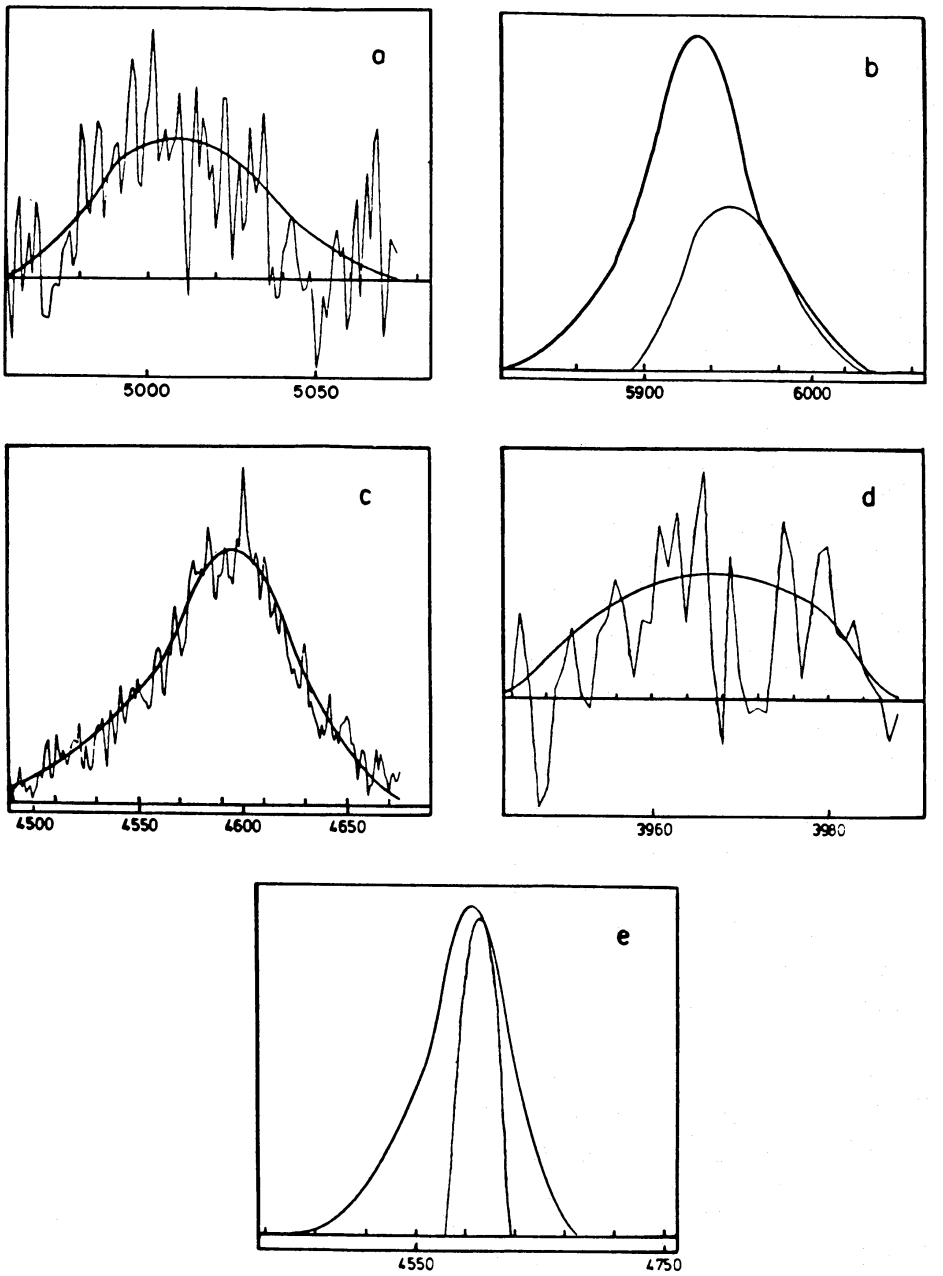

Figure 5. (a) The O I profile for Q0000 – 398 with cleaned version superposed. (b) Comparison of C IV (reinforced) and O I profiles of Q0000 – 398 scaled to match the red wings. (c) and (d) The observed profiles of C IV and C II for PKS 0304 – 392 with cleaned versions superposed. (e) Comparison of C IV (reinforced) and C II for PKS 0304 – 392.

possible. The superposition is typical of the sample and clearly demonstrates the shift between the two line peaks. In addition, although the FWHM of the O I feature is comparable to that of C IV, its wings appear to be substantially narrower. This was generally the case and implies a lower velocity dispersion for the O I emitting gas. However, the lower *S/N* in the O I profile is likely to contribute to this discrepancy.

In Fig. 5(c) and (d) the C IV and C II profiles of 0304 – 392 are displayed with the cleaned profiles superposed and in Fig. 5(e) C II (faint) is superposed upon C IV. A small shift is apparent between the line peaks in this QSO and C II appears narrower, although this may be due to the poor *S/N*. The other two available C II profiles behaved similarly but their

S/N was equally poor due to the weakness of the feature. If confirmed, the narrow width of the C II profile would imply that emission originates in a region distinct from the BLR. This is an exciting possibility since no NL component has yet been confirmed in the spectra of high-redshift QSOs.

Differing redshifts such as those reported here immediately pose the question of which lines, if any, give the true redshift of the QSO. It has been shown that Mg II λ 2798 is approximately at rest with respect to the narrow lines in low-redshift QSOs (Gaskell 1981; Wilkes 1982). It is expected that, should high-redshift QSOs possess a narrow-line region, its emission lines would also be redshifted $\sim 800\,\mathrm{km\,s^{-1}}$ relative to Lyα and the high-ionization lines. There is evidence in Seyfert 1 galaxies (Heckman *et al.* 1981; Whittle 1982) that the narrow lines are within $\sim 100\,\mathrm{km\,s^{-1}}$ of the underlying galaxy redshift. Extrapolation from high-redshift QSOs to Seyferts thus provides evidence that the low-ionization broad lines are indicators of the true redshift while the higher ionization lines are blueshifted.

5.3 C III] λ 1909

An immediate distinction between the C III] line profile and those of the other high-ionization lines is that it tends to be broader. This is apparent for the present sample in Table 5, in which the sample size, mean and standard deviation of the FWHM are tabulated for the strongest emission lines. A weak emission feature which may explain the width discrepancy has been reported to be blended into the blue wing of C III] at a rest wavelength of ~ 1860 Å (Wills *et al.* 1980; Baldwin & Netzer 1978). Competing possible identifications for this feature are Si III] λ 1892, Al III λ 1858 and a blend of Fe II multiplets with a mean wavelength ~ 1860 Å (Gaskell, Shields & Wampler 1981).

Table 5. Linewidth distribution parameters.

Emission Line	n	$\bar{x}$	σ
Lyαλ1215	10	4140	1200
NVλ1240	9	4750	1040
OIV]/SiIVλ1400	8	4750	760
CIVλ1549	12	3840	950
CIII]λ1909	7	5140	1790

In this sample four of the six C III] profiles have a blue asymmetry about their peak; in two of these, Q1101 – 264 and 2044 – 168, a partially resolved emission feature is apparent. The rest wavelength is ~ 1870 Å in both cases. The intensity relative to C III] was estimated in two ways, first by reflection of the red wing and subsequent subtraction of the resulting symmetric C III] profile and secondly by deblending using the C IV profile as a prototype. Strengths of 10 and 30 per cent C III] were found for Q1101 – 264 and 2044 – 168 respectively. In addition, the profile of 0304 – 392 is symmetric but there is a very noisy emission feature blueward of C III] with a central wavelength ~ 1864 Å in the rest frame (see Fig. 1). It is notable that these three QSOs are also those in which Fe II emission is apparent redward of C IV, tending to support the Fe II identification since emission in the two sets of ultraviolet multiplets is likely to be related.

Although the sample is small, one might expect a correlation between FWHM and the presence of a blue asymmetry for the C III] profile if the blended emission is solely responsible for the large widths. None is apparent and, in particular, the C III] profile of

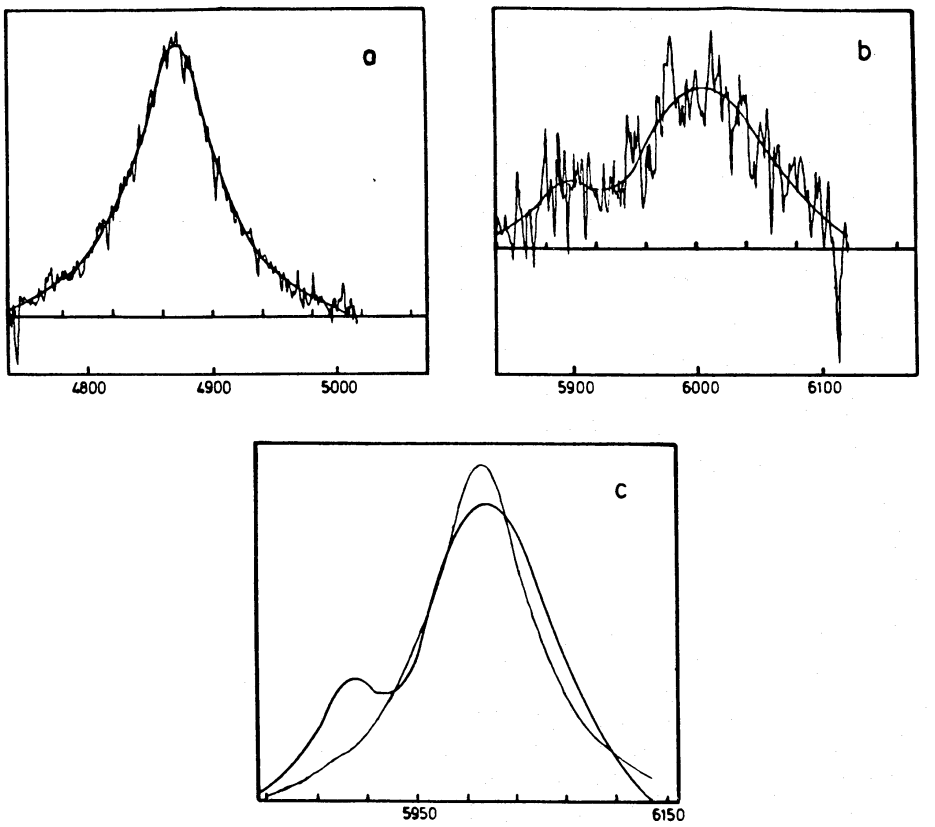

Figure 6. (a) and (b) The observed C IV and C III] profiles (respectively) for Q1101 – 264 with cleaned versions superposed. (c) Superposition of the C IV and C III] (reinforced) profiles.

0304 – 392 is significantly broader than the other profiles in the spectrum (Table 3) despite being resolved from the blended feature. Comparison of C IV and C III] line profiles after allowing for the presence of weak emission reveals a tendency for the C III] profile to have a relatively weaker peak and less extended wings. In Fig. 6(a) and (b) the observed C IV and C III] profiles of Q1101 – 264 are displayed with the cleaned versions superposed. In Fig. 6(c) the cleaned version of C III] is superposed upon that of C IV. Blended emission is clearly present in the blue wing of C III] and in addition the above mentioned differences between the profiles are apparent. Differences of this nature would tend to increase the measured FWHM of the profile in agreement with the observations. It should be noted that the lower *S/N* in C III] may also contribute.

Thus, this sample confirms earlier reports of an emission feature in the blue wing of C III]. The rest wavelength of ~ 1870 Å argues against the Si III] λ 1892 identification and there is some preference for Fe II over Al III λ 1858 since the Fe III emission redward of C IV may be related. This feature does not completely account for the observed large FWHM of C III] and there is evidence for intrinsic differences between the profiles of C IV and C III].

5.4 O VI λ 1034/Ly β λ 1026

There are four O VI/Ly β features present in this sample, one of which (that of Q2204 – 408) is badly contaminated by absorption lines and thus cannot be investigated in detail. In this QSO the majority of the emission lines have a strong blue asymmetry and the observed O VI/Ly β feature is consistent with its having a similar shape. The other three features were

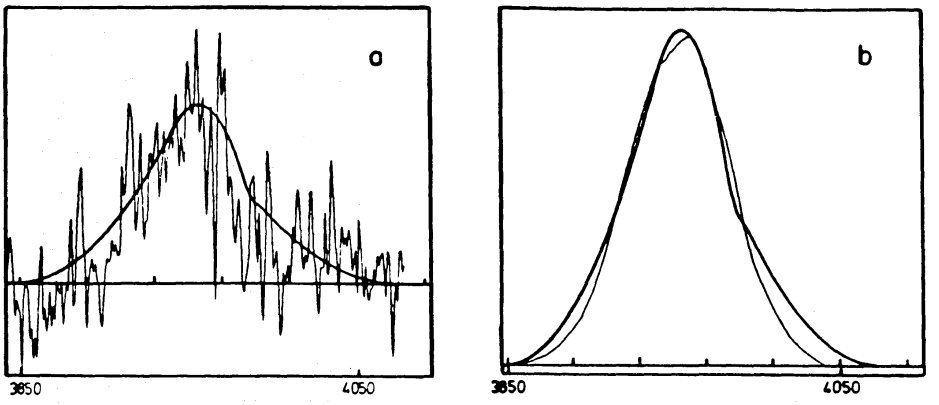

Figure 7. (a) Observed O VI/Lyβ emission profile for Q0000 – 398 with cleaned version superposed. (b) The cleaned O VI/Lyβ profile is shown (reinforced) with the synthesis superposed (see text).

deblended using the C IV profile in the same QSO, as described in Section 4. The feature in Q0207 – 398 showed no evidence for the presence of Lyβ emission, but in the other two the estimated contribution was substantial: $I(\text{Ly}\beta)/I(\text{O VI}) \sim 0.31$ for Q0000 – 398 and ~ 0.46 for 2212 – 299. In Fig. 7(a) the observed O VI emission line of Q0000 – 398 is displayed with the cleaned version superposed. A similar plot for C IV can be found in Fig. 2(a). In Fig. 7(b) the synthesis using the cleaned C IV profile is superposed (feint) upon the O VI/Lyβ profile with relative strengths as given above. It should be noted that, despite the poor *S/N* and heavy contamination by absorption lines in O VI/Lyβ feature, there is evidence in Fig. 7(b) that its wings are more extended than those of C IV, again implying subtle differences between the line profiles. However, another interpretation of the observed O VI profiles which cannot be ruled out is that there is a real difference between the profiles of C IV and O VI; although the existence of such a large discrepancy for O VI only seems unlikely unless the emission originates in a totally different region of the BLR.

5.5 LYMAN LINE EMISSION

As reported earlier, the observed Lyman line ratios were estimated as $I(\text{Ly}\beta)/I(\text{Ly}\alpha) \sim 0.06$ for Q0000 – 398; $0.06 < I(\text{Ly}\beta)/I(\text{Ly}\alpha) < 0.1$ and $I(\text{Ly}\beta)/I(\text{Ly}\alpha) \sim 0.05$ for 2212 – 299. The presence of higher order Lyman emission is unexpected for optically thick gas, in particular for a case B recombination model all Lyβ photons are degraded to Lyα + Hα. A number of mechanisms for the production of Lyβ and higher order Lyman line emission have been discussed in the literature. Netzer (1976) considered self-absorption at high optical depths in the Balmer lines and concluded that a ratio of Lyβ/Ly$\alpha \sim 0.07$ was probably a maximum under his assumed conditions. Kwan & Krolik (1981) include Bowen fluorescence, in which Lyβ pumps the $3d^3D^0$ state of O I, and conclude that the maximum ratio possible is ~ 0.1. The value predicted by their standard model is 0.02. An additional possibility is the presence of a component of gas which is optically thin in the Lyman lines, yielding line ratios with the normal case A recombination values. This is an important possibility, particularly in the light of the lack of any significant asymmetry in the Lyα profile (WC82), which may also suggest the presence of an optically thin component. However, problems with explaining the observed low Lyα/Hβ ratio would be enhanced.

On the basis of the small amount of data available, the observed Lyβ strength lies at the upper end of the range predicted by model calculations for optically thick gas. If thin gas is

present Lyγ is also expected. It is difficult to place limits upon its presence or absence owing to the high density of absorption lines in this spectral region and also to the proximity of C III λ 977. A feature has occasionally been detected in low-resolution data (e.g. Green *et al.* 1980) but it is impossible to distinguish between the two identifications or to deblend unless high-resolution data are obtained. Confirmation of the detection in 2212 – 299 of this sample, or in any other QSO spectrum, would have important implications on modelling of the photoionized emitting gas.

5.6 C IV ASYMMETRY

Of the nine C IV profiles included in this sample, six have a degree of blue asymmetry (e.g. see WC82 and Fig. 6a) and in only one (Q2204 – 408, perhaps also 0304 – 392) is this asymmetry apparent in the other lines. Of the remaining C IV profiles, three are accurately symmetric about their peak (e.g. Q0000 – 398, Fig. 3a) but one of these, 1331+170, is significantly blueshifted, i.e. with respect to the Lyα peak it is also blue asymmetric. Young, Sargent & Boksenberg (1982) report a similar result, finding that 20 out of 23 C IV profiles in their sample have an extended blue wing. In an attempt to discover the reason for such asymmetry, correlations of the skewness of these profiles, as measured by the Karl Pearson skew parameter, with other properties of the features, such as the intensity and equivalent width were looked for; none was found.

It should be noted that C IV is the only uncontaminated line profile in the spectra of high-redshift QSOs* and thus it is difficult to determine whether this asymmetry is peculiar to C IV or common to all the emission lines. In the profile comparisons reported in this paper, there is good evidence in only three cases that C IV and Lyα profiles are substantially different: Q0207 – 398, 1331+170 and 2044 – 168; in the third of these the Lyα profile has already been noted as abnormal (Section 3).

5.7 THE 1400 Å BLEND

The identity of this feature has long been a subject of contention; it it generally attributed to a blend of the doublet Si IV λ 1397 and the quintet O IV] λ 1402, the former being preferred until the correct mean wavelength of O IV] (1402 Å rather than 1406 Å) was pointed out by Wills & Netzer (1979). Their subsequent study of the distribution in published wavelengths for the feature implies that O IV] is the principal contributor to the line (~ 85 per cent), but the large variance in this distribution suggests that the relative proportions vary from QSO to QSO (see also Gaskell *et al.* 1981).

There are eight 1400 Å profiles available in this sample of QSO spectra. One of these is weak and too noisy to study in detail. The remaining seven were deblended in order to investigate the relative contributions of each component using the C IV profile in each case. Owing to the multiple nature of the two components, deblending was performed in two stages. First, individual synthetic blends of both the O IV] λ 1402 quintet and the Si IV λ 1397 doublet were generated using the C IV profile. The following relative strengths for the O IV] components were used: $\lambda\lambda$ 1397.2/1399.7/1401.16/1404.81/1407.39 = 0.1/1.0/5.0/2.0/1.0. (Flower & Nussbaumer 1975). Secondly, a synthesis of the final blend was formed from a combination of these two. Since C IV is also a doublet of comparable separation, generation of these blends using the C IV profile as a template is not strictly valid. However, C IV is the only available unblended line in this spectral region and thus provides the best approximation to the intrinsic profile of each component. In addition, since there is

* One possible blended feature is the Si II λ 1530 doublet, but it has a predicted strength of ~ 1/2 that of the triplet Si II λ 1814, which is not observed in QSO spectra, and thus is not believed to be detectable.

Table 6. Distribution in relative intensity of Si IV λ 1397 and O IV] λ 1402 emission in the observed blends.

Object	Peak wavelength/Å (rest frame)	I(SiIV) / I(OIV])	Notes
Q0207-398	1397.3	0.8	CIV has strong blue skew, SiIV likely an underestimate
0304-392	1402.0	0.12	
Q1101-264	1400.8	0.7	
1331+170	1402.1	0.6	Assuming neither feature shares blueshift of CIV
1559+089	1399.5	-	Too noisy, peak + ∿ 1
2044-168	1399.4	1.12	
Q2204-408	1404.9	0.0	
2212-299	1400.5	1.14	

no certainty that the intrinsic profiles are identical, any errors introduced are of the same nature as those already present in such a deblending procedure (Section 5 and WC82).

Table 6 shows the measured positions and intensity ratios of two contributors to the blend for the present sample of QSOs. It is clear that the ratios vary substantially from object to object with O IV] stronger on average (Si IV/O IV] ~ 0.6). Fig. 8(b) shows the superposition of synthetic blend (feint) upon the observed 1400 Å profile for Q1101 – 264; (see Fig. 8a and WC82 for original profiles). It should also be noted that, with one exception, the wings of the feature appear to be less extended than those of the C IV profile used in the synthesis.

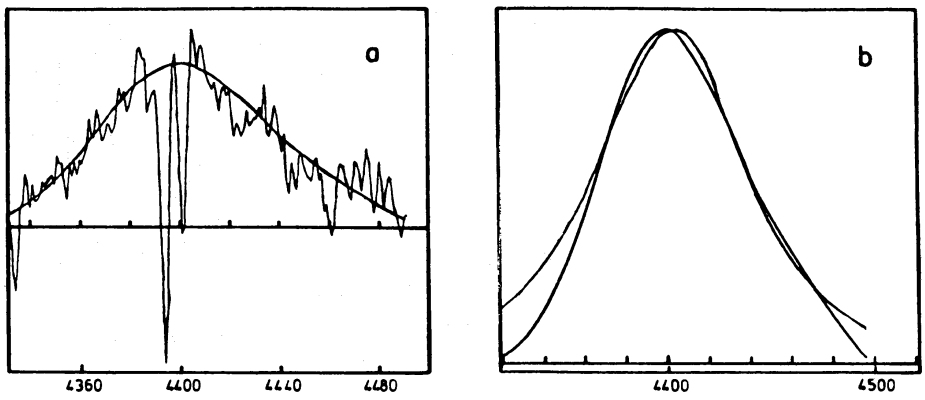

Figure 8. (a) The observed 1400 Å feature for Q1101 – 264 with cleaned version superposed. (b) Comparison of the 1400 Å feature (reinforced) with the synthesis generated using the C IV profile.

6 Discussion

As discussed earlier, the main aim of this study is to gain more information concerning the dynamics and geometrical configuration of the emitting gas in the BLR. The results presented so far which have relevant implications are as follows:

(1) The lack of any noticeable asymmetry in the Lyα profile when compared with the high-ionization lines. Such asymmetry is expected from any radially flowing gas distribution since the gas clouds are believed to be optically thick in Lyα (WC82).

(2) The blueshift of the Lyα and high-ionization line peaks with respect to the low-ionization lines and, probably, the QSO itself. This result implies the presence of radial flow and some form of obscuration in the BLR (see also Gaskell 1982).

(3) The tendency for C IV to have a blue asymmetric profile. It is certain that three of the C IV profiles in this sample have a substantially different shape from the corresponding Lyα line.

(4) The evidence for Lyβ emission blended with O VI λ 1304, in the spectra of Q0000 – 398 and 2212 – 299 and possibly Lyγ emission in the latter.

In addition, it has long been accepted that the line profiles are roughly logarithmic in shape (Blumenthal & Mathews 1975) and with similar widths, measured by the FWHM. This suggests that lines of very different ionization originate in similar areas of the BLR and has been the basis for using single zone photoionization models (Davidson & Netzer 1979). There is evidence from the present sample, though often marginal, that when studied in detail, profiles from different species differ systematically. In particular, the C IV profile is less strongly peaked and has weaker wings than the Lyα profile. There appears to be a tendency for the wings of the profiles to be more extended for progressively higher ionization lines, but with the Lyα wings being the most extended. These results imply that a single zone model is, at best, an approximation and re-emphasize the importance of profile studies.

There are two important points that should be noted at this stage. On the one hand the lack of any marked difference between the profile of Lyα and those of the high-ionization lines puts strong limits upon the amount of radial motion of optically thick gas in a single-component BLR (WC82). On the other hand, the observed shift between low- and high-ionization line peaks implies that the latter are strongly blue asymmetric with respect to the redshift of the parent object, while appearing, with the occasional exception of C IV, to be relatively symmetric about their line centres (Q2204 – 408 is a notable exception to this). The most straightforward explanation for such a shift is a combination of radial flow and obscuration. Clearly, if this is the explanation, a compromise is necessary in order to account for both the shifts and the lack of substantially different Lyα profiles.

6.1 ORBITAL MOTION

If the motion of these clouds were purely orbital, each cloud would move in a randomly directed orbit bound by its gravitational attraction to the central mass of the QSO, cloud velocity $\sim r^{-0.5}$, where r is the distance from the centre (virial theorem). There are several problems with such a model (see e.g. Shields 1978). First, there is no simple correspondence between the projected line-of-sight velocity of a cloud and its position in the cloud distribution and consequently systematic asymmetries or relative shifting of the emission lines cannot be produced unless the orbits are parabolic or highly elliptical with the cloud structure changing substantially and irreversibly within a single orbital period (Kwan & Carroll 1982). Even in this case any asymmetry is likely to be small and shifts probably do not result. Secondly, $v(r) \sim r^{-0.5}$ results in substantial differences in the linewidths of low- and high-ionization lines since, unless the radiation parameter is constant throughout the BLR, emission from atoms of differing ionization states issues from different areas of the BLR.

6.2 RADIAL FLOW

As briefly mentioned earlier, radial flow coupled with obscuration of the emission from areas of the BLR may combine to produce asymmetric profiles and/or an apparent shift of the emission lines involved, relative to the systemic velocity of the object. In order to produce shifting of certain lines only, in this case Lyα and the high-ionization lines, the

obscuration must be localized within the BLR. This leaves two alternative interpretations for the behaviour of the gas clouds in the BLR.

6.2.1 *Radial outflow combined with obscuration of emission from high-ionization clouds on the far-side of the central source*

In order to produce a blueshifted emission line, clouds on the near-side of the QSO must be brighter. This requires obscuration external to the clouds since internal obscuration would have the reverse effect.

One obvious possible source of obscuration is the presence of dust in the intercloud medium (ICM). It is most likely to exist in the outer regions of the BLR where the temperatures are lower and the gas clouds in these outer regions will be the most heavily obscured. In order to obscure the high-ionization lines only they must originate in the outer regions while the low-ionization lines come from smaller radii. This is possible if the gas density within the clouds decreases rapidly with distance from the central source such that the inner clouds are optically thick and emit mainly low-ionization lines, while the outer clouds are thinner. Emission from the low-ionization, inner clouds is affected only by dust in the outer regions on the near-side of the BLR, thus the whole distribution of inner clouds is affected similarly and there is no resultant shift of the emission lines. Problems may be encountered in making this model self-consistent since the presence of ICM dust will affect the ionizing radiation on route to the highly-ionized clouds.

An alternative form of obscuration is the presence of a large disc of gas and dust, probably an extension of gas accreting on to a central black hole. There are two alternatives: First, if the highly ionized gas is situated in the inner areas of the BLR, a significantly larger proportion of the high-ionization photons would be obscured by a thick disc of radius $\sim 10^{18}$ cm. Secondly, the highly ionized gas may be further away from the central source. A thin disc becoming thicker at $\sim 10^{18}$ cm radius, where it is cooler and may be gathering dust from the parent galaxy, would then preferentially obscure the highly ionized gas.

6.2.2 *A combination of radial inflow and obscuration of the emission from highly ionized clouds on the near-side of the central source*

Obscuration which is intrinsic to the clouds results in a phase function in the emitted intensity from individual clouds and thus, assuming a low covering factor (~ 5–10 per cent), the far-side clouds appear brighter, and inflow causes a blue asymmetric line (WC82). For the low-ionization lines not to be shifted, it is necessary either that the emitting clouds do not possess a phase function or that they do not share in the overall radial flow. They may be further from the central source and have a lower infall velocity, though with a velocity dispersion or orbital velocity component large enough to produce a FWHM comparable with that of the high-ionization lines.

It is apparent that, although radial motion may explain the blueshift of the high-ionization lines, the lack of a significant difference between the Lyα profile and that of the high-ionization lines is a strong argument against such motion in optically thick gas. As we have seen, thick gas is generally deemed necessary in order to generate the observed line ratios in a one or two zone photoionization model (Davidson & Netzer 1979). This is particularly a problem for radial outflow since the near-side clouds are preferentially seen and thus very little, if any, Lyα emission would be observed from optically thick clouds. However, for inflow models, obscuration within the emitting clouds may be dominated by dust so that a phase function is present for photons of all species. Additional line optical depth in Lyα may not change the phase function sufficiently to result in a unique line profile. Thus, if the gas clouds are optically thick, the second possibility of radial inflow

combined with internal obscuration seems marginally preferable, although it is more difficult to produce high velocities in an inflowing rather than outflowing model. Alternatively, if a large proportion of the Lyα photons originate in optically thin gas clouds, there would be no phase function in their emission, an asymmetric line would not be expected and the radial outflow option would be equally favourable (except that the Lyα/Hβ problem, Baldwin 1975, would be increased). Evidence for an optically thin component may be provided by the presence of Lyβ emission reported earlier.

Additional evidence for the inflow model is the relative position of Lyα and Hβ; the former tending to behave as a high-ionization line and the latter as a low. The most commonly accepted explanation for the low observed Lyα/Hβ line ratio, as compared with those expected for case B recombination, is that the Balmer emission is enhanced deep in the neutral regions of a cloud due to the thermalization of Lyα and the collisional excitation of Hβ. Kwan & Krolik (1981) find that the emissivity of the Balmer line increases toward the back of a cloud. If so, the Hβ emission from a cloud with intrinsic dust obscuration will remain fairly isotropic, in contrast with that of Lyα, C IV and the high-ionization lines which are biased toward the front of the cloud. Hβ photons would be observed from the whole cloud distribution while those from the far-side clouds would dominate the high-ionization lines. In the alternative model with external obscuration the Hβ emission must originate predominantly in the low-ionization region for the line not to be shifted.

7 Conclusions

There are many plausible models for the BLR which have not been mentioned in the above discussion, e.g. those involving cylindrical rotation or jets. The shortage of high-quality data on the emission line profiles results in a lack of observational constraints with which to test these competing models in a quantitative manner.

To date, the most important observational constraints which a model should be able to reproduce are the following:

(1) Fairly symmetric, logarithmic profiles in all emission lines, in particular Lyα.
(2) Blueshifting of high- relative to low-ionization lines.
(3) Reasonably high velocities throughout the BLR, any gradient being in the sense that low-ionization gas moves more slowly.
(4) Detectable emission in the higher order Lyman lines.
(5) The observed distribution of linewidths (Baldwin 1975; Wilkes 1982).
(6) The tendency for any asymmetries to be blue rather than red.

Observationally, more data are required so that study may be continued in many areas. In particular, more high-quality spectra would facilitate the study of profile asymmetries and intercomparisons across a larger sample and also a search for higher order Lyman line emission. It is especially important to make detailed comparisons of the profiles of high- and low-ionization lines either by obtaining ultra-high quality data around O I λ 1304 or observing Mg II λ 2798 in the red. (Fe II emission often present throughout the Mg II profile may cause too many problems.)

In addition to the above points, the following results have emerged from this study:

(1) C III] λ 1909 is blended with emission in its blue wing, the most likely identification being either Al III λ 1858 or Fe II λ 1860.
(2) The relative strengths of the contributors to the 1400 Å blend (O IV] λ 1402, Si IV λ 1397) vary across a sample of QSOs with O IV] generally being stronger.

Acknowledgments

It is my pleasure to thank my supervisor, Dr R. F. Carswell for his continued and invaluable support during the course of this research. In addition, he and his collaborators, Drs M. G. Smith, A. Boksenberg and J. A. J. Whelan very kindly allowed me to use and present data obtained by them for another project. I gratefully acknowledge the financial support of both an SERC Studentship and at present a NATO research fellowship.

I would also like to thank all my friends and colleages at Cambridge and Steward Observatory for helpful and enlightening discussion, in particular Professor R. J. Weymann, Drs C. B. Foltz, R. G. Carlberg, Professor C. Hazard, and Dr C. M. Gaskell. The QSO 1559+089 was discovered as part of an objective prism survey carried out by Professor Hazard and his collaborators in Cambridge, to whom I am grateful. I wish to thank the referee for his useful comments.

References

Atwood, B., Baldwin, J. A. & Carswell, R. F., 1982. *Astrophys. J.*, **257**, 559.
Baldwin, J. A., 1975. *Astrophys. J.*, **201**, 26.
Baldwin, J. A. & Netzer, H., 1978. *Astrophys. J.*, **226**, 1.
Baldwin, J. A., Burbidge, E. M., Hazard, C., Murdoch, H. S., Robinson, L. B. & Wampler, E. J., 1973. *Astrophys. J.*, **185**, 739.
Blumenthal, G. R. & Mathews, W. G., 1975. *Astrophys. J.*, **198**, 517.
Boksenberg, A., 1972. *Auxiliary Instruments for Large Telescopes*, Proceedings of ESO-CERN Conference, p. 295, eds Lnasten, S. & Reitz, A.
Boksenberg, A., 1978. *Proceedings, Symposium of 26th Plenary Meeting of COSPAR*, p. 929, eds van der Hucht, K. A. & Viana, G., Pergamon Press.
Burbidge, G. R. & Kinman, T. D., 1966. *Astrophys. J.*, **145**, 654.
Carswell, R. F. & Ferland, G. J., 1980. *Mon. Not. R. astr. Soc.*, **191**, 55.
Carswell, R. F., Hilliard, R. L., Strittmatter, P. A., Taylor, D. J. & Weymann, R. J., 1975. *Astrophys. J.*, **196**, 351.
Carswell, R. F., Whelan, J. A. J., Smith, M. G., Boksenberg, A. & Tytler, D., 1982. *Mon. Not. R. astr. Soc.*, 198, 91.
Collin-Souffrin, S., Joly, M., Heidman, N. & Dumont, S., 1979. *Astr. Astrophys.*, **72**, 293.
Davidson, K., 1972. *Astrophys. J.*, **171**, 213.
Davidson, K. & Netzer, H., 1979. *Rev. Mod. Phys.*, **51**, 715.
Flower, D. R. & Nussbaumer, H., 1975. *Astr. Astrophys.*, **45**, 145.
Gaskell, C. M., 1981. *PhD thesis*, University of California, Santa Cruz.
Gaskell, C. M., 1982. *Astrophys. J.*, **263**, 79.
Gaskell, C. M., Shields, G. A. & Wampler, E. J., 1981. *Astrophys. J.*, 249, 443.
Grandi, S. A., 1981. *Astrophys. J.*, **251**, 451.
Green, R. F., Fier, J. R., Schmidt, M., Estabrook, F. B., Lane, A. L. & Wahlquist, H. D., 1980. *Astrophys. J.*, 239, 483.
Heckman, T. M., Miley, G. K., van Breugel, W. J. M. & Butcher, H. R., 1981. *Astrophys. J.*, 247, 403.
Hewitt, A. & Burbidge, G. R., 1980. *Astrophys. J. Suppl.*, **43**, 57.
Jauncey, D. L., Wright, A. E., Peterson, B. A. & Condon, J. J., 1978. *Astrophys. J.*, **219**, L1.
Kwan, J. & Carroll, T. J., 1982. *Astrophys. J.*, **261**, 25.
Kwan, J. & Krolik, J. H., 1981. *Astrophys. J.*, 250, 478.
Netzer, H., 1976. *Mon. Not. R. astr. Soc.*, **177**, 473.
Oke, J. B., 1974. *Astrophys. J. Suppl.*, **27**, 21.
Osmer, P., 1979. *Astrophys. J.*, 227, 18.
Osmer, P. & Smith, M. G., 1976. *Astrophys. J.*, 210, 276.
Osmer, P. & Smith, M. G., 1977. *Astrophys. J.*, 213, 607.
Osmer, P. & Smith, M. G., 1980. *Astrophys. J. Suppl.*, 42, 333.
Peterson, B. M., Foltz, C. B. & Byard, P. L., 1981. *Astrophys. J.*, 251, 4.
Peterson, B. A., Jauncey, D. L., Wright, A. E. & Condon, J. J., 1976. *Astrophys. J.*, 207, L5.
Phillips, M. M., 1978a. *Astrophys. J. Suppl.*, **38**, 187.

Phillips, M. M., 1978b. *Astrophys. J.*, **226**, 736.
Shields, G., 1978. *Proc. Pitts. Conf. BL Lacs*, p. 257, ed. Wolfe, A. M.
Smith, M. G., 1976. *Astrophys. J.*, **206**, L125.
Smith, M. G., Carswell, R. F., Whelan, J. A. J., Wilkes, B. J., Boksenberg, A., Clowes, R. G., Savage, A. Cannon, R. D. & Wall, J. V., 1981. *Mon. Not. R. astr. Soc.*, **195**, 437.
Strittmatter, P. A., Carswell, R. F., Burbudge, E. M., Hazard, C., Baldwin, J. A., Robinson, L. & Wampler E. J., 1973. *Astrophys. J.*, **183**, 767.
Weymann, R. J., Williams, R. E., Peterson, B. M. & Turnshek, D. A., 1979. *Astrophys. J.*, **234**, 33.
Whelan, J. A. J., Smith, M. G. & Carswell, R. F., 1979. *Mon. Not. R. astr. Soc.*, **189**, 363.
Whittle, D. M., 1982. *PhD thesis*, University of Cambridge.
Wilkes, B. J., 1982. *PhD thesis*, University of Cambridge.
Wilkes, B. J. & Carswell, R. F., 1982. *Mon. Not. R. astr. Soc.*, **201**, 645.
Wills, D. & Netzer, H., 1979. *Astrophys. J.*, **233**, 1.
Wills, B. J., Netzer, H. & Wills, D., 1980. *Astrophys. J.*, **242**, L1.
Young, P. J., Sargent, W. L. W. & Boksenberg, A., 1982. *Astrophys. J. Suppl.*, **48**, 455.